



Article

Enhanced Activity of Hierarchical Nanostructural Birnessite-MnO₂-Based Materials Deposited onto Nickel Foam for Efficient Supercapacitor Electrodes

Shang-Chao Hung^{1,2}, Yi-Rong Chou³, Cheng-Di Dong⁴ , Kuang-Chung Tsai⁵ and Wein-Duo Yang^{3,*}

¹ Fuzhou Polytechnic, Fuzhou 350108, China; schung99@gmail.com

² Intelligent Technology Research Centre, Fuzhou 350108, China

³ Department of Chemical and Materials Engineering, National Kaohsiung University of Science and Technology, Kaohsiung 80778, Taiwan; mygirl850629@gmail.com

⁴ Department of Marine Environmental Engineering, National Kaohsiung University of Science and Technology, Kaohsiung 81157, Taiwan; cddong@nkust.edu.tw

⁵ Department of Safety, Health and Environmental Engineering, National Kaohsiung University of Science and Technology, Kaohsiung 82445, Taiwan; tsai kc@nkust.edu.tw

* Correspondence: ywd@nkust.edu.tw; Tel.: +886-7-3814526 (ext. 15116)

Received: 20 August 2020; Accepted: 25 September 2020; Published: 27 September 2020



Abstract: Hierarchical porous birnessite-MnO₂-based nanostructure composite materials were prepared on a nickel foam substrate by a successive ionic layer adsorption and reaction method (SILAR). Following composition with reduced graphene oxide (rGO) and multiwall carbon nanotubes (MWCNTs), the as-obtained MnO₂, MnO₂/rGO and MnO₂/rGO-MWCNT materials exhibited pore size distributions of 2–8 nm, 5–15 nm and 2–75 nm, respectively. For the MnO₂/rGO-MWCNT material in particular, the addition of MWCNT and rGO enhanced the superb distribution of micropores, mesopores and macropores and greatly improved the electrochemical performance. The as-obtained MnO₂/rGO-MWCNT/NF electrode showed a specific capacitance that reached as high as 416 F·g⁻¹ at 1 A·g⁻¹ in 1 M Na₂SO₄ aqueous electrolyte and also an excellent rate capability and high cycling stability, with a capacitance retention of 85.6% after 10,000 cycles. Electrochemical impedance spectroscopy (EIS) analyses showed a low resistance charge transfer resistance for the as-prepared MnO₂/rGO-MWCNT/NF nanostructures. Therefore, MnO₂/rGO-MWCNT/NF composites were successfully synthesized and displayed enhanced electrochemical performance as potential electrode materials for supercapacitors.

Keywords: hierarchical; birnessite-MnO₂; specific capacitance; electrochemical performance

1. Introduction

Recently, supercapacitors (SCs) have attracted widespread attention and research due to their advantages, such as high specific capacitance, high power density, good cycle life, and low maintenance cost [1–3]; however, the storage energy density for such devices is not as good as that found for lithium-ion batteries, which, thus, limits applications. In addition, the pore size, specific surface area, surface functional groups, and conductivity for an electrode active material can also affect the specific capacitance of a supercapacitor [4,5]. Therefore, improving nanostructure electrode materials with high specific capacitance to increase their specific capacitance and energy density is a focus of research for energy storage devices [6–8].

Manganese dioxide (MnO₂) has the advantages of low cost, high environmental safety and high theoretical capacitance (1380 F·g⁻¹) in aqueous electrolytes and is considered to be one of the most

promising capacitor materials [9,10]. The common crystal structures of MnO_2 are α , β , γ , δ and λ type crystal phases. The size of the pore structure in each crystal is different. At present, various crystal type structures have been widely studied. Among such structures, birnessite- MnO_2 (δ - MnO_2) is widely used as a positive active material for supercapacitors [11,12]. Devaraj et al. [13] pointed out that δ - MnO_2 has a MnO_6 octahedron structure due to the crystal sharing double bonds with the neighboring crystal lattice; the width of δ - MnO_2 is large enough to accommodate the insertion or removal of cations with a large ionic radius. Wolff et al. [14] published δ - MnO_2 as a two-dimensional layered structure, which can hold water and cations between a large number of sheet materials. Brousse et al. [15] studied the electrochemical properties of MnO_2 with different crystal structures. The results show that the layered α - MnO_2 and δ - MnO_2 can rapidly diffuse potassium ions to improve the capacitance performance. Ghodbane et al. [16] pointed out that δ - MnO_2 is more suitable for the insertion and removal of ions, and shows ionic conductivity and increased electrical properties.

According to the principles of ion adsorption-desorption and intercalation, the electrochemical capacitance behavior mainly occurs on the surface layer of the manganese dioxide electrode material. Therefore, increasing the specific surface area can effectively improve the utilization of the active material, resulting in a higher specific capacitance. However, the application of MnO_2 in electrodes still shows some shortcomings, such as low conductivity, which severely limits the application value [17]. Fortunately, this weakness can be improved by introducing high-conductivity carbon materials into electrode materials [18]. In recent years, reduced graphene oxide (rGO) has been shown to exhibit excellent electronic, capacitance, and mechanical properties, chemical stability, and a high specific surface area. It is often compounded with metal oxides and used as an electrode material for supercapacitors [19,20]. It is worth mentioning that the aggregation and restacking of particles during the electrode preparation process for graphene results in a significant decrease in electrochemical performance. Therefore, by combining graphene and multiwall carbon nanotubes (MWCNTs), one can obtain graphene/MWCNT composite materials, which exhibit a unique structure that has attracted the attention of researchers. This composite material containing graphene and carbon nanotubes shows good electrical conductivity and excellent chemical stability, which can effectively promote the electron transfer properties of the electrolyte in the electrode material [21,22]. Particularly, MnO_2 composited with MWCNT and graphene can effectively improve the material aggregation in the electrode and improve the performance of the supercapacitor.

Successive ionic layer adsorption and reaction (SILAR) is a chemical solution deposition technology. Using this method can coat the required thickness of film on the substrate, which is a simple process [23,24]. Jana et al. [25] prepared MnO_2 cathode materials on stainless steel substrates by hydrothermal method or SILAR technology, respectively. Graphene particles were deposited on nanocarbon cloth as anodes to fabricate rGO- MnO_2 asymmetric supercapacitors. It indicated that the rGO- MnO_2 material synthesized by hydrothermal method had serious agglomeration, which reduced the conductivity and surface area of the electrode. On the contrary, the cathode material made by SILAR technology had a high surface area and a higher diffusion rate of electrolyte. Moreover, the SILAR process not only prevents the aggregation of graphene, but also eliminates the necessity of nonconductive organic binders and carbon black in the process to reduce the manufacturing cost of supercapacitor electrodes. The SILAR method is used in rGO- MnO_2 composite films, which can manufacture a lightweight and ultrasmall super capacitor. Jadhav et al. [26], who also studied SILAR technology, used stainless steel as the substrate and immersion in manganese ion solutions by the SILAR technology. It was shown that the prepared MnO_2 film was an amorphous particle, which exhibited an electrochemical oxidation-reduction reaction during charge and discharge. SILAR technology can uniformly adhere $\text{Mn}_3\text{O}_4/\text{GO}$ to the substrate, and at $5 \text{ mV}\cdot\text{s}^{-1}$, the specific capacitance is $344 \text{ F}\cdot\text{g}^{-1}$. However, to the best of our knowledge, utilizing the SILAR process to fabricate δ - MnO_2 -based electrode materials has been very scarce and is worthy of study.

In this study, an environmentally friendly and low-cost process was developed to produce high-performance supercapacitor electrode materials. SILAR was used to prepare MnO_2 -based

composite electrode materials on nickel foam (NF), such as MnO_2/NF , $\text{MnO}_2/\text{rGO}/\text{NF}$ and $\text{MnO}_2/\text{rGO-MWCNT}/\text{NF}$ composite cathode materials to improve the agglomeration for such electrode materials. The specific surface area, pore size and distribution for the electrode materials were studied, and mixtures of rGO and MWCNT with different weight ratios were studied to investigate the electrochemical properties of the composite electrodes.

2. Materials and Methods

2.1. Materials

Analytical-grade chemicals were used as received, without any further purification. Nickel foam (98% purity, Fluka, Tokyo, Japan), graphene oxide sheet (99% purity, Goal Bio, Hsichu, Taiwan), multiwalled carbon nanotube (MWCNT) (98% purity, Showa, Tokyo, Japan), sodium sulfate ($\geq 98\%$ purity, Honeywell, Hannover, Germany), safranin (99% purity, Alfa Aesar, Karlsruhe, Germany), potassium permanganate (98% purity, Showa, Tokyo, Japan), and manganese sulfate (98% purity, Showa, Tokyo, Japan) were used for the preparation of the MnO_2 -based/NF electrode. Sodium sulfate ($\geq 98\%$ purity, Honeywell, Hannover, Germany) was used as the electrolyte.

2.2. Preparation of MnO_2 -Based/NF Electrode

A graphene sheet weighing 0.25 g was weighed and added into 50 mL DI water. After ultrasonic mixing for 1 h, ammonia water was used to adjust the pH at approximately 11. Then, the as-prepared GO suspension was put in an autoclave and kept at 180 °C for 12 h. After cooling, the suspension solution was turned into rGO. Finally, it was dried in a freeze dryer for 24 h. The properties of the as-obtained materials were characterized (Supplementary Materials, Figure S1).

The nickel foam (1 cm \times 1 cm) was washed with acetone, ultrasonic vibration, and deionized water, and then dried. Then, 0.5 mg mL^{-1} of safranin was mixed in DI water with an initial mixture of rGO and MWCNT at a concentration of 0.6 mg $\cdot \text{mL}^{-1}$ in DI water. The weight ratio for rGO and MWCNT was 1:1. The mixture was then subjected to an ultrasonic vibrator for 30 min to form a uniform suspension rGO-MWCNT ink.

The cleaned NF was immersed in reduced graphene oxide (rGO), MWCNT or dispersed rGO-MWCNT ink, and then rinsed with deionized water for 40 s to obtain rGO, MWCNT or rGO-MWCNT adhered to the NF substrate to prepare rGO/NF, MWCNT/NF or rGO-MWCNT/NF, respectively.

SILAR technology was used to coat the film onto the substrate. NF, rGO/NF, MWCNT/NF or rGO-MWCNT/NF was respectively placed into Mn^{2+} solution (0.01 M MnSO_4 solution) and MnO_4^- solution (0.01 M KMnO_4 solution), and then rinsed and air-dried. Mn^{2+} was oxidized and deposited layer by layer, which then underwent a redox reaction with MnO_4^- . Through the SILAR process, MnO_2 , MnO_2/rGO , $\text{MnO}_2/\text{rGO-MWCNT}$ was attached to the Ni substrate, respectively. This procedure was repeated five times. Finally, the as-deposited electrode was annealed at 200 °C for 1 h. Figure 1 shows a schematic for the preparation of $\text{MnO}_2/\text{rGO-MWCNT}/\text{NF}$ material via the successive ion layer adsorption and reaction method.

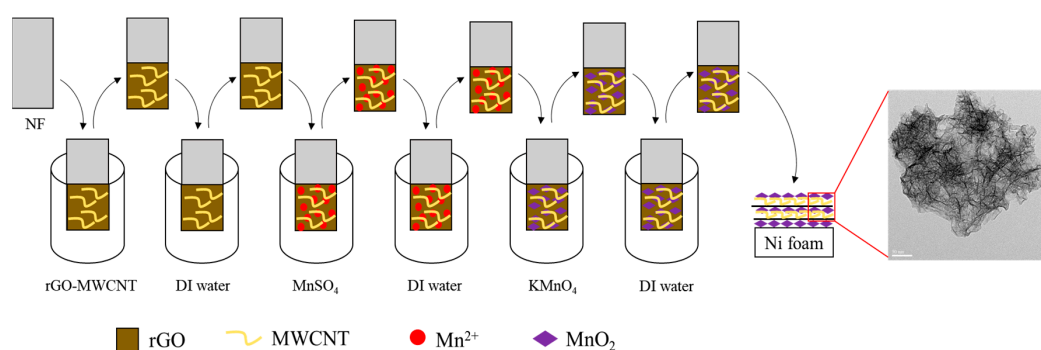


Figure 1. Schematic for the preparation of $\text{MnO}_2/\text{rGO-MWCNT}/\text{NF}$ electrode via the successive ion layer adsorption and reaction method.

2.3. Characterization

The crystal phases for the samples were examined using X-ray diffraction (XRD, Bruker, D8 ADVANCE, Karlsruhe, Germany) with $\text{Cu K}\alpha$ radiation ($\lambda = 1.5406 \text{ \AA}$). Furthermore, transmission electron microscopy (TEM) (JEOL, TEM-3010, Tokyo, Japan) with an acceleration voltage of 80 kV was utilized to examine the microstructures for the as-prepared MnO_2 -based electrodes. The Brunauer-Emmett-Teller (BET) surface area, Barrett-Joyner-Halenda (BJH) mesopore area, t-plot micropore area, and N_2 adsorption-desorption isotherms were measured with a Micrometrics ASAP 2020 instrument.

2.4. Electrochemical Characterization of the As-Obtained MnO_2 -Based/NF Electrodes

All the electrochemical properties were investigated using a conventional three-electrode electrochemical cell equipped with the as-prepared MnO_2 -based/NF electrode ($1.0 \text{ cm} \times 1.0 \text{ cm}$) as the working electrode, a platinum plate ($1.0 \text{ cm} \times 1.0 \text{ cm}$) as the counter electrode, and an Ag/AgCl as the reference electrode, and a $1.0 \text{ M Na}_2\text{SO}_4$ aqueous solution as the electrolyte.

Cyclic voltammetry (CV) and galvanostatic charging-discharging (GCD) tests were performed using a CHI 760D electrochemical workstation (CH Instruments, Inc., Austin, TX, USA).

The specific capacitance can be evaluated by the CV test using the following Formula (1):

$$C = \frac{Q}{V \times m \times \Delta U} \quad (1)$$

where Q is the area of the CV curve, V is the scan rate ($\text{V}\cdot\text{s}^{-1}$), m is the mass of the electrode active material (g), and ΔU is the voltage range (V).

The specific capacitance was obtained according to the discharge curve of the GCD test by using the Formula (2):

$$C_m = \frac{i \times \Delta t}{\Delta V \times m} \quad (2)$$

where i (A) is the discharge current, Δt (s) is the discharge time, ΔV (V) is the discharging potential difference, and m (g) is the mass of the loaded active material (MnO_2).

Electrochemical impedance spectra (EIS) were measured at open-circuit voltage, with a bias of 10 mV for frequencies ranging from 100 kHz to 0.01 Hz, to analyze the electron transport properties.

3. Results and Discussion

3.1. Characterization of the MnO_2 -Based Electrode Materials

The deposition of thin films was done by the following the steps to grow nucleation sites, and then ions reacted to produce the as-deposited material on the substrate, in the SILAR process. In this

case, Mn^{2+} from manganese sulfate was adsorbed on the nickel foam and reacted with MnO_4^- from potassium permanganate to produce MnO_2 .

In the preliminary experiment, MnO_2 prepared under different manganese ion concentrations was characterized by XRD, BET, CV and GCD analyses. The results showed that $\delta\text{-MnO}_2$ crystals were obtained at a lower concentration of MnSO_4 (0.01 M), and $\gamma\text{-MnO}_2$ crystals were prepared at concentrations of MnSO_4 higher than 0.05 M. Because $\delta\text{-MnO}_2$ crystal possessed a larger BET specific surface area and better pore properties, it exhibited better electrochemical characteristics (Supplementary Materials, Figure S2), therefore, preparation of $\delta\text{-MnO}_2$ was conducted on 0.01 M MnSO_4 in this study.

Figure 2 shows the XRD analysis for the MnO_2 -based electrode materials prepared by the SILAR process. The results show that a weak diffraction peak can be mainly attributed to the prepared sample, which indicates low crystallinity. Nevertheless, it can still be clearly found that the diffraction peaks at 2θ values of 37.2° and 66.8° were due to the (111) and (020) crystal planes of the birnessite-type MnO_2 (JCPDS 18-0802, Joint Committee on Powder Diffraction Standards (JCPDS), Newtown Square, PA, USA) [27] and that the peak width of the peak intensity was not strong. It is revealed that the MnO_2 material prepared by the SILAR method was not highly crystalline and that the crystallinity was not perfect. A clear diffraction peak was observed at a 2θ value of 22° for the as-deposited MnO_2/rGO material, showing the presence of rGO [28]; the small peak on the right of 22° , indicates that a small amount of unreacted graphite carbon existed in the GO. According to XRD analysis for the as-deposited $\text{MnO}_2/\text{rGO}\text{-MWCNT}/\text{NF}$ electrode material, the diffraction peak observed at a 2θ value of approximately 22° was characteristic of rGO; the peak observed at a 2θ value of approximately 25° was the characteristic peak for the MWCNTs. By using Bragg's Law, $n\lambda = 2d \sin\theta$, the interplanar spacing for rGO and MWCNT was calculated to be 0.40 nm and 0.36 nm, respectively.

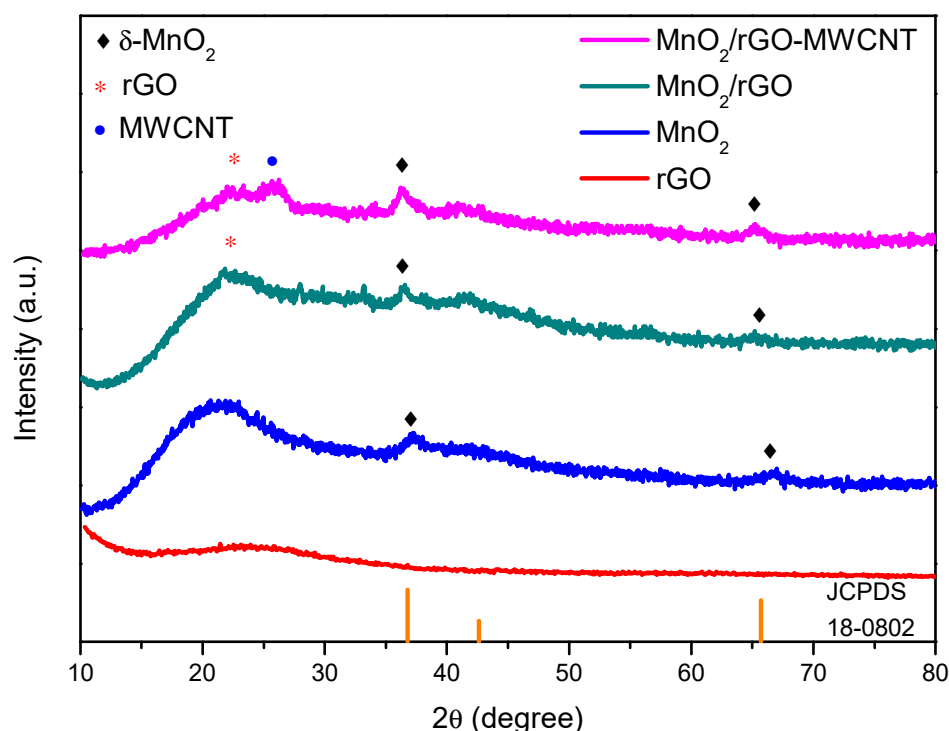


Figure 2. The X-ray diffraction (XRD) analysis for the MnO_2 -based electrode materials prepared by the successive ionic layer adsorption and reaction (SILAR) process.

Birnessite MnO_2 has a two-dimensional (2D) layered structure, consisting of MnO_6 octahedrons shared with edges. The spacing of this layered structure is approximately 7 \AA and it is located in the middle layer area, which is considered to be favorable for the transport of metal ions or water [29].

The specific capacitance of the relatively open layered structure of δ -MnO₂ is much higher than that of β -MnO₂ and γ -MnO₂ [30]. A detailed comparison of the XRD diffraction peaks for the three different electrode materials composed of MnO₂ (such as the two diffraction peaks at 2θ values of 37.2° and 66.8°) shows that the diffraction peak due to the MnO₂/rGO-MWCNT/NF electrode material broadened and shifted to a low diffraction angle; it can be presumed that the addition of MWCNT widened the crystal planes in the prepared electrode structure (such as the (111) and (020) crystal planes).

TEM was used to study the morphologies of the MnO₂-based materials. Figure 3 shows the TEM analysis for the as-obtained MnO₂, MnO₂/rGO and MnO₂/rGO-MWCNT materials. As shown in Figure 3a,b, it can be clearly seen that the prepared MnO₂ layered structure was loosely arranged. In addition, the selected region electron diffraction image shows an indistinct electron diffraction ring (upper right corner of Figure 3a), indicating that the prepared MnO₂ had poor crystallinity.

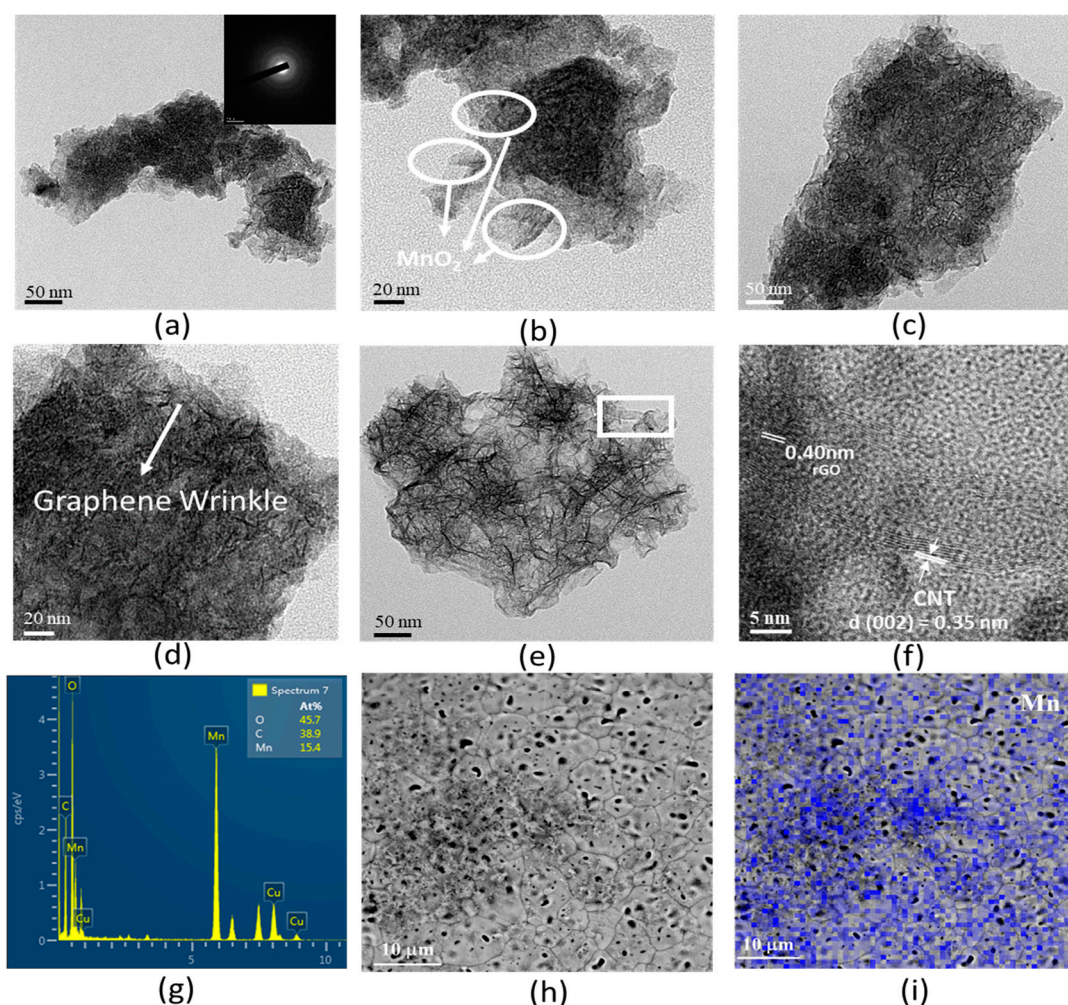


Figure 3. The TEM analysis for the as-obtained MnO₂ material (a,b), MnO₂/rGO (c,d) and MnO₂/rGO-MWCNT material (e,f), EDS of MnO₂/rGO-MWCNT/NF material (g), SEM and mapping of MnO₂/rGO-MWCNT/NF material (h,i), respectively.

TEM analysis of the MnO₂/rGO/NF nanocomposite electrode is shown in Figure 3c,d. Wrinklelike features for graphene can be observed. Because the MnO₂/rGO/NF was prepared by the SILAR process, the graphene could restack, resulting in excessive surface agglomeration, so it was difficult to observe the regular structure of MnO₂.

Figure 3e,f shows the TEM analysis for the prepared MnO₂/rGO-MWCNT/NF nanocomposite electrode. It indicated that the surface of the film showed 3D flowerlike structures staggered

with each other (Supplementary Materials, Figure S3). The flowerlike hierarchical nanostructure maintains good integrity because the CNTs prevent rGO from restacking; therefore, the prepared $\text{MnO}_2/\text{rGO-MWCNT/NF}$ materials have more uniform dispersion and homogeneity [31]. Following examination by high-resolution TEM, the lattice patterns for rGO and MWCNT were observed, which showed the interplanar spacing for rGO and MWCNT to be approximately 0.40 nm and 0.35 nm, respectively. This result is very consistent with the XRD results discussed in the previous section.

Furthermore, it was also found that the MWCNTs attach to the inside of MnO_2 , which indicates structural stability for the $\text{MnO}_2/\text{rGO-MWCNT/NF}$ nanocomposite electrode. Such an electrode structure can shorten the ion/electron transport length between the electrode and the electrolyte and increase the contact surface area. The 3D hierarchical flowerlike $\text{MnO}_2/\text{rGO-MWCNT/NF}$ nanocomposite electrode can be expected to show an excellent electrochemical performance. The energy dispersive spectrum (EDS) (Figure 3g) indicates that the $\text{MnO}_2/\text{rGO-MWCNT}$ material is composed of Mn, Ni, O and C, elements, except for Cu from the supporting Cu grid. It exhibits that the atomic composition of Mn and C is 15.4 at. % and 38.9 at. %, respectively; means that the loading amount of MnO_2 in the $\text{MnO}_2/\text{rGO-MWCNT}$ material is approximately 74 wt. %. Furthermore, the Mn element in the electrode dispersed well in the hybrid material (Figure 3h,i), indicating that MnO_2 has good dispersibility in the rGO-MWCNT. BET specific surface area and pore size distribution analysis for MnO_2 , MnO_2/rGO and $\text{MnO}_2/\text{rGO-MWCNT}$ materials scraped from the as-deposited electrodes is shown in Figure 4. Figure 4a shows the N_2 isotherm adsorption-desorption analysis for the MnO_2 -based materials. The results show a typical type IV isotherm. The sample has a clear triangular hysteresis loop and a step absorption between 0.4–0.9 P/P_0 , showing highly interconnected holes, and the material has a narrow opening and a wide structure [32].

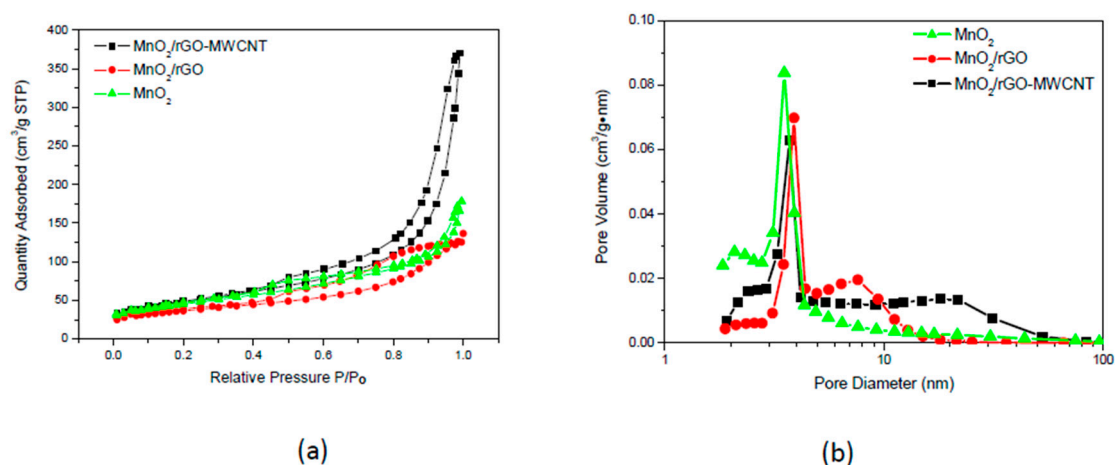


Figure 4. BET specific surface area and pore size distribution analysis for MnO_2 , MnO_2/rGO and $\text{MnO}_2/\text{rGO-MWCNT}$ materials. (a) N_2 isotherm adsorption-desorption analysis and (b) pore distribution analysis.

Table 1 shows the powder properties of MnO_2 , MnO_2/rGO and $\text{MnO}_2/\text{rGO-MWCNT}$ materials. For the table, the specific surface area and pore size distribution were obtained by using the BET equation; the pore volume and the average pore diameter were obtained from the branch-curves for the adsorption isotherm according to the Barrett–Joyner–Halenda (BJH) equation. The results show that the BET specific surface areas for the MnO_2 , $\text{MnO}_2/\text{MWCNT}$, MnO_2/rGO , and $\text{MnO}_2/\text{rGO-MWCNT}$ materials were $155.7 \text{ m}^2 \cdot \text{g}^{-1}$, $102.6 \text{ m}^2 \cdot \text{g}^{-1}$, $132.8 \text{ m}^2 \cdot \text{g}^{-1}$, and $167.7 \text{ m}^2 \cdot \text{g}^{-1}$, respectively and that the BJH pore sizes were 4.6 nm, 5.6 nm, 6.7 nm, and 13.6 nm, respectively. $\text{MnO}_2/\text{rGO-MWCNT}$ showed the largest BET specific surface area, which is attributed to the loosely arranged structure; the MnO_2/rGO specific surface area is small because graphene restacks.

Table 1. The powder properties of MnO₂, MnO₂/MWCNT, MnO₂/rGO and MnO₂/rGO-MWCNT materials.

Materials	Surface Area (m ² ·g ⁻¹)	Pore Volume (cm ³ ·g ⁻¹)	Pore Size (nm)
MnO ₂	155.7	0.4	4.6
MnO ₂ /MWCNT	102.6	0.3	5.6
MnO ₂ /rGO	132.8	0.2	6.7
MnO ₂ /rGO-MWCNT	167.7	0.5	13.6

In contrast, the MnO₂/rGO exhibits the smallest specific surface area. It can be explained by combined with the results of Raman shifts (Supplementary Materials, Figure S1). It indicates that the relative intensity ratio of the D-band to G-band, defined as $R = I_D/I_G$, of the commercial GO sheet was found to be 0.86. This indicates that the GO showed the characteristic of high regularity and low randomness. Then, the as-obtained rGO by the hydrothermal method showed a highly stacked sp² structure because of the elimination of the oxygen-containing functional groups, causing an increase in the reduction of graphite and a shift in the G band to 1585.5 cm⁻¹.

Furthermore, the R-value of MnO₂/rGO material increased after the SILAR process. That was presumably because some impurities and defects were introduced during the preparation. Moreover, the composited MnO₂ particles also damaged the graphene order. Additionally, in the preparation of MnO₂/rGO material, rGO was sequentially immersed in the MnSO₄ and KMnO₄ solutions by the SILAR process. Due to the high ionic strength of the solutions, the graphene was restacked and more agglomerated, resulting in specific surface area decrease.

Figure 4b shows the pore distribution analysis for MnO₂, MnO₂/rGO and MnO₂/rGO-MWCNT materials. It can be seen from the figure that the pore distributions for the three different electrode materials were 2–8 nm, 5–15 nm and 2–75 nm, respectively. Due to the wide distribution of the MnO₂/rGO-MWCNT material composition, it indicates the existence of a hierarchical porous structure. Especially for the MnO₂/rGO-MWCNT material, the addition of MWCNT and rGO enhances the superb distribution of micropores, mesopores and macropores, and greatly improves the electrochemical performance.

The electrolyte ions' size and the porous structure of the electrode are the key factors for the specific capacitance. The small size of the pores confines the accessible pores for the ions from the electrolyte solution. Su et al. [33] indicated that it is very important to meet the balance between the pore size and the ion size of the electrolyte for supercapacitors. However, an electrode material with hierarchical pore structure and high ion-accessible surface area that is helpful to ion transportation, and leading to high capacitance. It has been previously indicated that an ideal electrode material should have a hierarchical porous structure consisting of large pores (greater than 50 nm) used as an ion buffer reservoir, mesopores (2–50 nm) used for ionic migration and micropores (less than 2 nm) used for charge storage [34].

Xu et al. [35] also studied the supercapacitive properties of MnO₂ electrode in Li₂SO₄, Na₂SO₄ and K₂SO₄ electrolyte, respectively. They indicated that the charging-discharging rate can be affected by the size of the cation, the size of the hydrated cation, the mobility of the cation, and the adsorption-desorption rate. The lithium ion (Li⁺) and hydrated lithium ion (Li_h⁺) radius was 0.69 Å and 6 Å, respectively; sodium ion (Na⁺) and hydrated sodium ion (Na_h⁺) radius was 1.02 Å and 4 Å, respectively, and potassium ion (K⁺) and hydrated potassium ion (K_h⁺) radius was 1.38 Å and 3 Å, respectively. Therefore, Na⁺ ion may possess a moderate diffusion rate in MnO₂ matrix, a moderate adsorption-desorption rate, and a moderate mobility in aqueous solutions, resulting in the large capacitance and fast charging/discharging rate.

Thus, in the as-obtained MnO₂/rGO-MWCNT material, MWCNT helps prevent rGO from restacking and increases the specific surface area. The material has a highly hierarchical porous structure, which provides effective transportation for electrons and ions. MnO₂/rGO-MWCNT/NF as

an electrode in Na_2SO_4 electrolyte exhibits the higher specific capacitance as shown on Section 3.2 electrochemical properties.

3.2. Electrochemical Properties

These MnO_2 -based/NF materials were directly manufactured into working electrodes without using a binder to reveal their capacitance performance as shown in Figure 5. Figure 5a shows the analysis for the CV characteristics obtained for MnO_2/NF , $\text{MnO}_2/\text{MWCNT}/\text{NF}$, $\text{MnO}_2/\text{rGO}/\text{NF}$ and $\text{MnO}_2/\text{rGO-MWCNT}/\text{NF}$ in a 1 M Na_2SO_4 electrolyte at a scan rate of 5 mV s^{-1} , respectively.

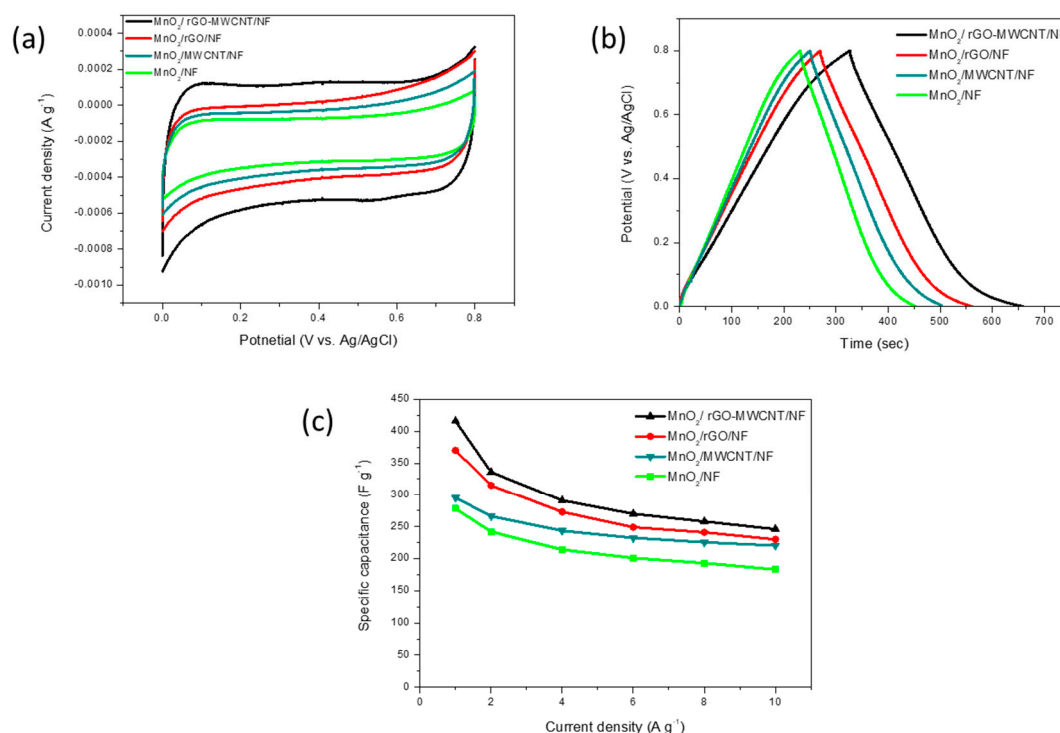


Figure 5. The capacitance performance of the as-deposited electrodes. (a) Cyclic voltammetry (CV) characteristics in a 1 M Na_2SO_4 electrolyte at a scan rate of $5 \text{ mV} \cdot \text{s}^{-1}$, (b) galvanostatic charging-discharging (GCD) characterization at $1 \text{ A} \cdot \text{g}^{-1}$; and (c) the relationship between the specific capacitance and current density from GCD examination.

The figure indicates the different electrodes with quasi-rectangular and quasi-symmetric CV curves. Among them, the area enclosed by the CV curve for the $\text{MnO}_2/\text{rGO-MWCNT}/\text{NF}$ electrode is much larger than the curve areas for the MnO_2/NF , $\text{MnO}_2/\text{MWCNT}/\text{NF}$ and $\text{MnO}_2/\text{rGO}/\text{NF}$ nanocomposite materials, showing that the $\text{MnO}_2/\text{rGO-MWCNT}/\text{NF}$ electrode had an extremely high specific capacitance.

In the CV curve, MnO_2/NF , $\text{MnO}_2/\text{MWCNT}/\text{NF}$ and $\text{MnO}_2/\text{rGO}/\text{NF}$ shows obvious gradient patterns in the voltage ranges of 0.0 V to 0.1 V and 0.7 to 0.8 V, individually, while the curve for the $\text{MnO}_2/\text{rGO-MWCNT}/\text{NF}$ can be observed to show an almost vertical CV characteristic curve with a near rectangular and symmetrical shape, indicating that the conductivity of $\text{MnO}_2/\text{rGO-MWCNT}/\text{NF}$ was greatly improved by the homogeneous mixing of rGO and MWCNT with MnO_2 , demonstrating excellent electrochemical performance. In addition, the CV curve areas for $\text{MnO}_2/\text{rGO-MWCNT}/\text{NF}$ are much larger than the CV curve areas for the $\text{MnO}_2/\text{rGO}/\text{NF}$, $\text{MnO}_2/\text{MWCNT}/\text{NF}$ and MnO_2/NF composites, respectively. It is speculated that both MnO_2 and MWCNT can be used as spacers to prevent aggregation of rGO, which is conducive towards obtaining a higher electric double layer capacitance for rGO. Furthermore, rGO and MWCNT act as electronic conduction channels to increase

the conductivity of MnO₂. This is proved by the EIS analysis below, which shows a low contact electrical resistance for the MnO₂/rGO-MWCNT/NF electrode.

Na₂SO₄ was used as electrolyte in this study, and the MnO₂-based/NF electrodes showed a quasi-rectangular shape in CV curves measured at different scan rates, indicating the capacitance characteristics for the MnO₂ deposited onto the NF electrode [36]. The CV curve for the MnO₂-based electrode in Na₂SO₄ electrolyte is unlike that expected from an electric double-layer capacitor (EDLC); the CV characteristic curve for an EDLC shows a nearly ideal rectangle [37]. The quasirectangular shape observed for the CV curve is a characteristic of the reversible surface redox reaction of MnO₂, the oxidation of Mn(III) to Mn(IV) and the reduction from Mn(IV) to Mn(III) [38].

Figure 5b shows GCD characterization for the as-obtained MnO₂/NF, MnO₂/MWCNT/NF, MnO₂/rGO/NF and MnO₂/rGO-MWCNT/NF electrodes at 1 A·g⁻¹. The longer discharge time of the MnO₂/rGO-MWCNT/NF electrode indicates that its capacitance was higher than that of the MnO₂/NF, MnO₂/MWCNT/NF and MnO₂/rGO/NF electrodes, which is consistent with the results obtained from CV tests. In particular, compared with the as-prepared electrodes, the MnO₂/rGO-MWCNT/NF electrode exhibits highly linear and almost symmetrical charge and discharge curves, revealing that the IR potential drop for MnO₂/rGO-MWCNT/NF is less noticeable. The as-obtained MnO₂/rGO-MWCNT/NF electrode has a maximum specific capacitance of 416 F·g⁻¹ at a low current density of 1 A·g⁻¹. Figure 5c further compares the relationship between the specific capacitance and current density determined from GCD examination. It can be found that, as the current density increases, the capacitance retention for the MnO₂/rGO-MWCNT/NF electrode was better than that for the MnO₂/NF, MnO₂/MWCNT/NF and MnO₂/rGO/NF electrodes. At a high current density of 10 F·g⁻¹, the specific capacitance of the MnO₂/rGO-MWCNT/NF electrode remained at 250 F·g⁻¹, while the MnO₂/NF, MnO₂/MWCNT/NF and MnO₂/rGO/NF electrodes showed a capacitance of 176 F·g⁻¹, 215 F·g⁻¹ and 232 F·g⁻¹, respectively.

There was no oxidation peak/reduction peak in the CV curves and the GCD discharge curve of 0.0–0.2 V indicates a similar characterization of slope variation of the time for the as-deposited MnO₂-based electrode as Na₂SO₄ used for electrolyte (Figure 5a,b). This is due to the charge transfer reaction between MnO₂ and Na₂SO₄ electrolyte, which is related to the pseudo-capacitance behavior [39].

Contrast to the MnO₂ electrode in KOH electrolyte, the oxidation peak/reduction peak appears in the CV curve, and the steep slope at the end of the GCD discharge curve [40]. It reported that redox reaction peaks were visible (in the CV curves), indicating that the process of energy storage was mainly associated with a pseudocapacitance mechanism and not the reaction between the Mn⁴⁺ and OH⁻ in the electrolyte [41]. The redox mechanism of MnO₂ in KOH electrolyte are reversible insertion/extraction of K⁺ in MnO₂ as Formula (3) [42]:



Figure 6 shows the cycling charge-discharge test for the MnO₂/NF, MnO₂/rGO/NF and MnO₂/rGO-MWCNT/NF electrodes in a 1 M Na₂SO₄ electrolyte at a constant current of 4 A·g⁻¹. The results clearly show that the specific capacitance of the MnO₂/rGO-MWCNT/NF electrode decreased at 10,000 cycles of charging and discharging; however, this decrease was smaller than that found for the MnO₂/rGO/NF and MnO₂/NF electrodes, respectively. The MnO₂/NF, MnO₂/MWCNT/NF, MnO₂/rGO/NF and MnO₂/rGO-MWCNT/NF electrodes exhibit a capacitance retention of 62.4% (from 194 to 121 F·g⁻¹), 78.8% (from 201 to 158 F·g⁻¹), 80.2% (from 223 to 179 F·g⁻¹), and 85.6% (from 302 to 259 F·g⁻¹), respectively.

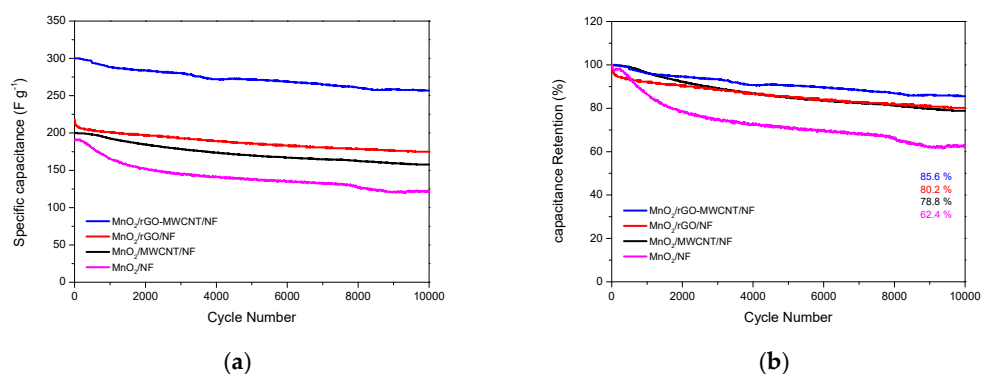


Figure 6. The cycling charge-discharge test for the as-deposited electrodes in a 1 M Na₂SO₄ electrolyte at a constant current of 4 A·g⁻¹. (a) Specific capacitance change and (b) capacitance retention.

In this study, SILAR technology was used to prepare a MnO₂/rGO-MWCNT/NF electrode onto rGO-MWCNT composite coated foamed nickel substrates. The material was found to show excellent cycle stability, which verifies that the charge storage reaction of the supercapacitor is reversible and that the electroactive material is stably adsorbed onto the substrate (current collector). MnO₂/rGO-MWCNT/NF can maintain high cyclic stability, which can be mainly attributed to the synergy effect between rGO, MWCNT and MnO₂.

Kong et al. [43] indicated that in the use of graphene nanosheets (GNS) to produce electrode materials, the aggregation and restacking of GNS will hinder the migration of electrolyte ions onto the interface, resulting in a substantial decrease in electrochemical performance. When multiwall carbon nanotubes (MWCNTs) are introduced, the graphene layer can be dispersed and the diffusion coefficient for the ions in the material can be effectively improved. In addition, the synergy effect between GNS and MWCNT is conducive to increasing the contact area between the electrode material and the electrolyte, providing a rich electroactive site for pseudocapacitance; such a hierarchical porous structure can effectively shorten the Na⁺ diffusion path. Sun et al. [44] studied a MnO₂/rGO/Ni composite foam electrode exhibiting good supercapacitor performance. It was pointed out that this excellent performance was closely related to the inherent hierarchical nanostructured porous MnO₂/rGO composite material grown onto the foamed Ni framework.

In this study, the SILAR process was used to apply layer-by-layer coating technology to prepare MnO₂/rGO-MWCNT/NF electrodes. In addition to the aforementioned characteristics [43,44], SILAR is more capable of producing a high surface area material with a higher electrolyte diffusion rate; in addition, rGO-MnO₂ electrodes prepared using SILAR technology can be used to manufacture lightweight and ultrasmall supercapacitor devices. It can induce the material to be more uniformly dispersed, increasing the capacity to build MnO₂/rGO-MWCNT/NF electrodes that demonstrate excellent cycle durability and excellent electrochemical performance.

To study the electrochemical mechanism for the MnO₂-based composite electrode materials showing good supercapacitor properties, MnO₂/NF, MnO₂/MWCNT/NF, MnO₂/rGO/NF and MnO₂/rGO-CNT/NF electrodes were prepared and subjected to EIS analysis, as shown in Figure 7. EIS measurements were taken in the frequency range from 100 kHz to 0.01 Hz. The results were displayed using Nyquist plots, which are divided into three different regions:

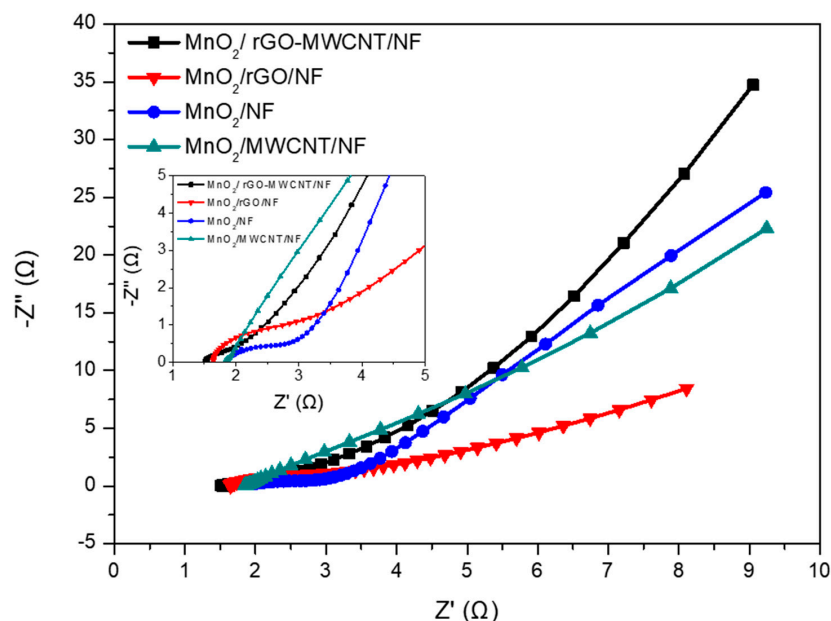


Figure 7. Electrochemical impedance spectra (EIS) analysis of the as-deposited electrodes in the frequency range from 100 kHz to 0.01 Hz.

In the high frequency region, the intercept at the real axis (Z_0) represents the equivalent series resistance (ESR), including the ionic resistance of the electrolyte, the inherent resistance of the substrate, and the contact resistance of the active material/current collector interface [45]. The span of the semicircular arc in the mid-high frequency region represents the charge transfer resistance (R_{ct}) at the electrode/electrolyte interface, also known as the Faraday resistance [46,47]. In the low-frequency region, the impedance represents the diffusion resistance for the electrolyte ions in the holes of the electrode. If the impedance graph increases sharply and tends to become a vertical line, a characteristic of pure capacitance behavior is indicated [48].

As shown in Figure 7, at high frequencies, the intercepts (R_E) for the curve and real axis for the $\text{MnO}_2/\text{rGO-MWCNT/NF}$ composite electrode, $\text{MnO}_2/\text{rGO/NF}$, $\text{MnO}_2/\text{MWCNT/NF}$ and MnO_2/Ni electrodes were determined to be 1.5 Ω , 1.7 Ω , 1.9 Ω and 2.1 Ω , representing a good contact between the electrode and the electrolyte, respectively. Especially, the $\text{MnO}_2/\text{rGO-MWCNT/NF}$ composite electrode shows the smallest equivalent resistance, demonstrating that the electrode has better conductivity. In particular, the as-obtained $\text{MnO}_2/\text{rGO-MWCNT/NF}$ composite electrode shows a vanishing semicircular arc-shaped impedance in the high-medium frequency region, indicating that the charge transfer resistance (R_{ct}) for the electrode is extremely low and that the ion diffusion path is very short. This result has hardly been observed previously in the high-to-medium frequency region, which is similar to the study of Liu et al. [49].

In the low-frequency region, the $\text{MnO}_2/\text{rGO-MWCNT/NF}$ electrode shows a straight line with a steep slope, indicating that the capacitance performance is very close to that of an ideal supercapacitor [50]. Additionally, in this region, the slope of the impedance curve for the $\text{MnO}_2/\text{rGO/NF}$ electrode is not as steep as that for the other electrodes, which may be due to the relatively worse dispersion of the rGO in the $\text{MnO}_2/\text{rGO/NF}$ electrode.

In this study, the as-obtained $\text{MnO}_2/\text{rGO-MWCNT/NF}$ electrode exhibited an extremely low impedance, which is attributed to the high homogeneity and nanostructure of the hierarchical porous composites grown on the nickel foam. The addition of MWCNTs leads to high aggregation but high specific surface area rGO is easily dispersed, unclogging the electronic conductive channels, resulting in an extremely small (even difficult to observe) arc span for the $\text{MnO}_2/\text{rGO-MWCNT/NF}$ electrode. In addition, the porous hierarchical structural $\text{MnO}_2/\text{rGO-MWCNT/NF}$ electrode exhibits an equivalent series resistance (R_E) that is lower than that of the other electrodes. This result further shows that

the composite MnO₂/rGO-MWCNT/NF electrode has faster kinetics compared to the MnO₂/rGO/NF, MnO₂/MWCNT/NF and MnO₂/NF composite electrode, which is beneficial towards improving the capacitance performance of the composite material, especially at high charge/discharge rates for the supercapacitor [51,52].

In addition, comparing the electrochemical properties of MnO₂/MWCNT/NF and MnO₂/rGO/NF electrodes, it is found that MnO₂/rGO/NF exhibits relatively good specific capacitance; however, the capacitance retention of MnO₂/MWCNT/NF electrode seems to be relatively stable. It is postulated that in the MnO₂/rGO/NF electrode, the MnO₂ nanoparticles make the rGO exhibit relatively good exfoliations, which makes the MnO₂ deposition relatively dispersed, and the material has a higher specific surface area. The electrode possesses a better pore structure makes Na₂SO₄ electrolyte easily adsorbed on the electrode, which facilitates migration and diffusion; resulting in a larger CV curve area and a higher specific capacitance value. In contrast, in MnO₂/MWCNT/NF, it is possible that MnO₂ is relatively easy to firmly adhere to the wall of the MWCNT, and the electrode microstructure is relatively strong, therefore, the capacitance retention during the charge-discharge cycling is relatively stable. However, the detailed differences between MnO₂/MWCNT/NF and MnO₂/rGO/NF need to be studied more accurately.

Table 2 shows a comparison of electrochemical performance of MnO₂-based electrode in the literatures [6,53–56]. Galvanostatic charge-discharge measurement results revealed that the composite with hybrid MnO₂/rGO-CNT exhibited the specific capacitance of 416 F·g⁻¹ at 1 A·g⁻¹ in a 1 M Na₂SO₄ electrolyte and an excellent capacitance retention of 85.6% at 10,000 charge-discharge cycles. The capacitance retention is quite higher than that of the previously studied electrode material.

Table 2. Comparison of electrochemical performance of MnO₂-based electrode in the literatures.

Material	Electrolyte	Current Density (A/g)	Capacitance Retention (%)	Specific Capacitance (F/g)	Ref.
MnO ₂	0.5 M Na ₂ SO ₄	1		336	[53]
MnO ₂ /rGO	1 M Na ₂ SO ₄	0.5	94.7 (1000 cycles)	288	[6]
MnO ₂ /rEGO	1 M Na ₂ SO ₄	0.5	90.3 (1000 cycles)	99.5	[54]
δ-MnO ₂ /GO	1 M Na ₂ SO ₄	1	81 (1000 cycles)	255	[55]
MnO ₂ /CNTs	1 M Na ₂ SO ₄	0.2	90 (2000 cycles)	162	[56]
MnO ₂ /rGO-CNT	1 M Na ₂ SO ₄	1	85.6 (10,000 cycles)	416	This work

rEGO: reduced graphene oxide obtained from electrochemical exfoliation method.

Combining the above results, the hybrid nanostructural rGO-MWCNT and MnO₂ material on nickel foam enables fast electron and ion transportation and further improves electrochemical performance. The addition of MWCNTs leads to high aggregation but also to the easy dispersion of rGO. The 3D network structure of the MnO₂/rGO-MWCNT/NF electrode was found to exhibit an excellent pore distribution, which can facilitate passage of electrons, charge storage and electron transportation. Therefore, MnO₂/rGO-MWCNT/NF composites were successfully synthesized, which display enhanced electrochemical performance as potential electrode materials for supercapacitors.

4. Conclusions

SILAR technology was used to construct 3D δ-MnO₂-based/foamed nickel electrodes. A hierarchical porous MnO₂ nanocomposite electrode material was supported on rGO-coated and rGO-MWCNT-coated nickel foam by convenient and simple “immersion and drying”, respectively. Because MWCNTs can effectively enable rGO to form a stable dispersion, they are beneficial for the uniform deposition of MnO₂ onto the substrate.

The synergetic combination of rGO-MWCNT and pseudocapacitance MnO₂ material onto nickel foam enables fast electron and ion transportation and further improves electrochemical performance. The as-prepared MnO₂/rGO-MWCNT/NF electrode was found to exhibit extremely low impedance due to the high uniformity and nanostructured material properties of the porous composite material grown onto the nickel foam. The addition of MWCNTs leads to high aggregation but also to the easy dispersion of high specific surface area rGO. The 3D network structure of the MnO₂/rGO-MWCNT/NF

electrode was found to exhibit an excellent pore distribution, which can facilitate passage of electrons, charge storage and electron transportation.

The as-deposited MnO₂/rGO-MWCNT/NF hierarchical porous nanostructural electrode exhibited a high specific capacitance of 416 F·g⁻¹ at 1 A·g⁻¹ in 1 M Na₂SO₄. After 10,000 charge and discharge cycles, the capacitance retention reached 85.6%. Therefore, this high-performance and convenient fabrication method provides excellent prospects for energy storage applications.

Supplementary Materials: The following are available online at <http://www.mdpi.com/2079-4991/10/10/1933/s1>, Figure S1: Properties of the as-obtained materials; Figure S2: Material properties and electrochemical characterization of the as-obtained MnO₂ from different concentrations of MnSO₄; Figure S3: FESEM images for the as-obtained MnO₂-based/NF materials.

Author Contributions: W.-D.Y., conceived and designed the experiments; Y.-R.C., performed the experiments; C.-D.D. and K.-C.T., analyzed the data; and S.-C.H. wrote the paper. All authors have read and agreed to the published version of the manuscript.

Funding: This research was funded by the Ministry of Science and Technology of Taiwan for its financial support under grant no. MOST-106-2221-E-151-040.

Conflicts of Interest: The authors declare no conflict of interest.

References

1. Afif, A.; Rahman, S.M.; Azad, A.T.; Zaini, J.; Islan, M.A.; Azad, A.K. Advanced materials and technologies for hybrid supercapacitors for energy storage—A review. *J. Energy Storage* **2019**, *25*, 100852–100876. [CrossRef]
2. Borenstein, A.; Strauss, V.; Kowal, M.D.; Yoonessi, M.; Muni, M.; Anderson, M.; Kaner, R.B. Laser-reduced graphene-oxide/ferrocene: A 3-D redox-active composite for supercapacitor electrodes. *J. Mater. Chem.* **2018**, *A6*, 20463–20472. [CrossRef]
3. Muzaffar, A.; Ahamed, M.B.; Deshmukh, K.; Thirumalai, J. A review on recent advances in hybrid supercapacitors: Design, fabrication and applications. *Renew. Sustain. Energy Rev.* **2019**, *101*, 123–145. [CrossRef]
4. Yang, P.; Ding, Y.; Lin, Z.; Chen, Z.; Li, Y.; Qiang, P.; Ebrahimi, M.; Mai, W.; Wong, C.P.; Wang, Z.L. Low-cost high-performance solid-state asymmetric supercapacitors based on MnO₂ nanowires and Fe₂O₃ nanotubes. *Nano Lett.* **2014**, *14*, 731–736. [CrossRef] [PubMed]
5. Zhi, M.; Xiang, C.; Li, J.; Li, M.; Wu, N. Nanostructured carbon-metal oxide composite electrodes for supercapacitors: A review. *Nanoscale* **2013**, *5*, 72–88. [CrossRef] [PubMed]
6. Zhao, Z.Y.; Shen, T.; Liu, Z.H.; Zhong, Q.S.; Qin, Y.J. Facile fabrication of binder-free reduced graphene oxide/MnO₂/Ni foam hybrid electrode for high-performance supercapacitors. *J. Alloys Compd.* **2020**, *812*, 152124–152133. [CrossRef]
7. Fan, Z.; Yan, J.; Wei, T.; Zhi, L.; Ning, G.; Li, T.; Wei, F. Asymmetric supercapacitors based on graphene/MnO₂ and activated carbon nanofiber electrodes with high power and energy density. *Adv. Funct. Mater.* **2011**, *21*, 2366–2375. [CrossRef]
8. Lei, R.; Zhang, H.; Lei, W.; Li, D.; Fang, Q.; Ni, H.W.; Gu, H.Z. MnO₂ nanowires electrodeposited on freestanding graphenated carbon nanotubes as binder-free electrodes with enhanced supercapacitor performance. *Mater. Lett.* **2019**, *249*, 140–142. [CrossRef]
9. Li, M.; Zu, M.; Yu, J.; Cheng, H.; Li, Q. Stretchable fiber supercapacitors with high volumetric performance based on buckled MnO₂/oxidized carbon nanotube fiber electrodes. *Small* **2017**, *13*, 1–7. [CrossRef]
10. Lv, Z.; Luo, Y.; Tang, Y.; Wei, J.; Zhu, Z.; Zhou, X.; Li, W.; Zeng, Y.; Zhang, W.; Zhang, Y.; et al. Editable supercapacitors with customizable stretchability based on mechanically strengthened ultralong MnO₂ nanowire composite. *Adv. Mater.* **2018**, *30*, 1–9. [CrossRef]
11. Li, Y.; Jian, J.; Xiao, L.; Liu, F.; Cheng, G.; Sun, M.; Zhou, J. Electrostatic self-assembly deposition of manganese dioxide nanosheets on functionalized graphene sheets as supercapacitor electrode. *Ceram. Int.* **2018**, *44*, 2269–2273.
12. Zhao, G.; Zhang, D.; Zhang, L.; Sun, K. Ti@δ-MnO₂ core-shell nanowire arrays as self-supported electrodes of supercapacitors and Li ion batteries. *Electrochim. Acta* **2016**, *202*, 8–13.
13. Devaraj, S.; Munichandraiah, N. Effect of crystallographic structure of MnO₂ on its electrochemical capacitance properties. *J. Phys. Chem. C* **2008**, *112*, 4406–4417.
14. De Wolff, P.M. Interpretation of some γ-MnO₂ diffraction patterns. *Acta Cryst.* **1959**, *12*, 341–345.

15. Brousse, T.; Toupin, M.; Dugas, R.; Athouel, L.; Crosnier, O.; Belanger, D. Crystalline MnO₂ as possible alternatives to amorphous compounds in electrochemical supercapacitors. *J. Electrochem. Soc.* **2006**, *153*, 2171–2180.
16. Ghodbane, O.; Pascal, J.; Favier, F. Microstructural effects on charge-storage properties in MnO₂-based electrochemical supercapacitors. *ACS Appl. Mater. Interfaces* **2009**, *1*, 1130–1139.
17. Cakici, M.; Kakarla, R.R.; Alonso-Marroquin, F. Advanced electrochemical energy storage supercapacitors based on the flexible carbon fiber fabric-coated with uniform coral-like MnO₂ structured electrodes. *Chem. Eng. J.* **2017**, *309*, 151–158.
18. Dong, J.; Lu, G.; Wu, F.; Xu, C.; Kang, X.; Cheng, Z. Facile synthesis of a nitrogen-doped graphene flower-like MnO₂ nanocomposite and its application in supercapacitors. *Appl. Surf. Sci.* **2018**, *427*, 986–993.
19. Ding, Y.; Zhang, N.; Zhang, J.; Wang, X.; Jin, J.; Zheng, X.; Fang, Y. The additive-free electrode based on the layered MnO₂ nanoflowers/reduced, graphene oxide film for high performance supercapacitor. *Ceram. Int.* **2017**, *43*, 5374–5381.
20. Wang, B.; Ruan, T.T.; Chen, Y.; Jin, F.; Peng, L.; Zhou, Y.; Wang, D.L.; Dou, S.X. Graphene-based composites for electrochemical energy storage. *Energy Storage Mater.* **2020**, *24*, 22–51.
21. Cheng, Q.; Tang, J.; Ma, J.; Zhang, H.; Shinya, N.; Qin, L.-C. Graphene and carbon nanotube composite electrodes for supercapacitors with ultra-high energy density. *Phys. Chem. Chem. Phys.* **2011**, *13*, 17615–17624. [[CrossRef](#)] [[PubMed](#)]
22. Fan, Z.; Yan, J.; Zhi, L.; Zhang, Q.; Wei, T.; Feng, J.; Zhang, M.; Qian, W.; Wei, F. A three-dimensional carbon nanotube/graphene sandwich and its application as electrode in supercapacitors. *Adv. Mater.* **2010**, *22*, 3723–3728. [[CrossRef](#)] [[PubMed](#)]
23. Kovacı, H.; Akaltun, Y.; Yetim, A.F.; Çelik, Y.U.A. Investigation of the usage possibility of CuO and CuS thin films produced by successive ionic layer adsorption and reaction (SILAR) as solid lubricant. *Surf. Coat. Technol.* **2018**, *344*, 522–527. [[CrossRef](#)]
24. Liu, Y.; Luo, D.; Shi, K.; Michaud, X.; Zhitomirsky, I. Asymmetric supercapacitor based on MnO₂ and Fe₂O₃ nanotube active materials and graphene current collectors. *Nano-Struct. Nano-Objects* **2018**, *15*, 98–106. [[CrossRef](#)]
25. Jana, M.L.; Saha, S.J.; Samanta, P.N.; Murmu, N.C.; Kim, N.H.; Kuila, T.; Lee, J.H. A successive ionic layer adsorption and reaction (SILAR) method to fabricate a layer-by-layer (LbL) MnO₂-reduced graphene oxide assembly for supercapacitor application. *J. Power Sources* **2017**, *340*, 380–392. [[CrossRef](#)]
26. Jadhav, P.R.; Shinde, V.V.; Navathe, G.J.; Karanjkar, M.M.; Patil, P.S. Manganese oxide thin films deposited by SILAR method for supercapacitor application. *Aip. Conf. Proc.* **2013**, *1536*, 679–680.
27. Ji, C.; Ren, H.; Yan, S. Control of manganese dioxide crystallographic structure in the redox reaction between graphene and permanganate ions and their electrochemical performance. *RSC Adv.* **2015**, *5*, 21978–21987. [[CrossRef](#)]
28. Qiao, X.; Liao, S.; You, C.; Chen, R. Phosphorus and nitrogen dual doped and simultaneously reduced graphene oxide with high surface area as efficient metal-free electrocatalyst for oxygen reduction. *Catalysts* **2015**, *5*, 981–991. [[CrossRef](#)]
29. Zhao, S.; Liu, T.; Hou, D.; Zeng, W.; Miao, B.; Hussain, S.; Peng, X.; Javed, M.S. Controlled synthesis of hierarchical birnessite-type MnO₂ nanoflowers for supercapacitor applications. *Appl. Surf. Sci.* **2015**, *356*, 259–265. [[CrossRef](#)]
30. Zhang, X.; Yu, P.; Zhang, H.; Zhang, D.; Sun, X.; Ma, Y. Rapid hydrothermal synthesis of hierarchical nanostructures assembled from ultrathin birnessite-type MnO₂ nanosheets for supercapacitor applications. *Electrochim. Acta* **2013**, *89*, 523–529. [[CrossRef](#)]
31. Zhu, S.; Li, L.; Liu, J.; Wang, H.; Wang, T.; Zhang, Y.; Zhang, L.; Ruoff, R.S.; Dong, F. Structural directed growth of ultrathin parallel birnessite on β-MnO₂ for high-performance asymmetric supercapacitors. *ACS Nano* **2018**, *12*, 1033–1042. [[CrossRef](#)] [[PubMed](#)]
32. Tsai, Y.-C.; Yang, W.-D.; Lee, K.-C.; Huang, C.-M. An effective electrodeposition mode for porous MnO₂/Ni foam composite for asymmetric supercapacitors. *Materials* **2016**, *9*, 246. [[CrossRef](#)] [[PubMed](#)]
33. Su, H.; Zhang, H.; Liu, F.; Chun, F.; Zhang, B.; Chu, X.; Huang, H.; Deng, W.; Gu, B.; Zhang, H.; et al. High power supercapacitors based on hierarchically porous sheet-like nanocarbons with ionic liquid electrolytes. *Chem. Eng. J.* **2017**, *322*, 73–81. [[CrossRef](#)]
34. Hao, P.; Zhao, Z.; Tian, J.; Li, H.; Sang, Y.; Yu, G.; Cai, H.; Liu, H.; Wong, C.P.; Umar, A. Hierarchical porous carbon aerogel derived from bagasse for high performance supercapacitor electrode. *Nanoscale* **2014**, *6*, 12120–12129. [[CrossRef](#)] [[PubMed](#)]
35. Xu, C.; Li, B.; Du, H.; Kang, F.; Zeng, Y. Supercapacitive studies on amorphous MnO₂ in mild solutions. *J. Power Sources* **2008**, *184*, 691–694. [[CrossRef](#)]

36. Athouël, L.; Moser, F.; Dugas, R.; Crosnier, O.; Bélanger, D.; Brousse, T. Variation of the MnO₂ birnessite structure upon charge/discharge in an electrochemical supercapacitor electrode in aqueous Na₂SO₄ electrolyte. *J. Phys. Chem. C* **2008**, *112*, 7270–7277. [[CrossRef](#)]
37. Barzegar, F.; Momodu, D.Y.; Fashedemi, O.O.; Bello, A.; Dangbegnon, J.K.; Manyala, N. Investigation of different aqueous electrolytes on the electrochemical performance of activated carbon-based supercapacitors. *RSC Adv.* **2015**, *5*, 107482–107487. [[CrossRef](#)]
38. Simon, P.; Gogotsi, Y. Materials for electrochemical capacitors. *Nat. Mater.* **2008**, *7*, 845–854. [[CrossRef](#)]
39. Gund, G.S.; Dubal, D.P.; Patil, B.H.; Shinde, S.S.; Lokhande, C.D. Enhanced activity of chemically synthesized hybrid graphene oxide/Mn₃O₄ composite for high performance supercapacitors. *Electrochim. Acta* **2013**, *92*, 205–215. [[CrossRef](#)]
40. Lin, L.; Tang, S.; Zhao, S.; Peng, X.; Hu, N. Hierarchical three-dimensional FeCo₂O₄@MnO₂ core-shell nanosheet arrays on nickel foam for high-performance supercapacitor. *Electrochim. Acta* **2017**, *228*, 175–182. [[CrossRef](#)]
41. Li, D.; Meng, F.; Yan, X.; Yang, L.; Heng, H.; Zhu, Y. One-pot hydrothermal synthesis of Mn₃O₄ nanorods grown on Ni foam for high performance supercapacitor applications. *Nanoscale Res. Lett.* **2013**, *8*, 535. [[CrossRef](#)]
42. Bi, Y.; Nautiyal, A.; Zhang, H.; Luo, J.; Zhang, X. One-pot microwave synthesis of NiO/MnO₂ composite as a high-performance electrode material for supercapacitors. *Electrochim. Acta* **2018**, *260*, 952–958.
43. Kong, S.; Cheng, K.; Ouyang, T.; Gao, Y.; Ye, K.; Wang, G.; Cao, D. Facile dip coating processed 3D MnO₂-graphene nanosheets/MWNT-Ni foam composites for electrochemical supercapacitors. *Electrochim. Acta* **2017**, *226*, 29–39.
44. Sun, Y.; Zhang, W.; Li, D.; Gao, L.; Hou, C.; Zhang, Y.; Liu, Y. Facile synthesis of MnO₂/rGO/Ni composite foam with excellent pseudocapacitive behavior for supercapacitors. *J. Alloys Compd.* **2015**, *649*, 579–584.
45. Kumar, A.; Sanger, A.; Kumar, A.; Kumar, Y.; Chandra, R. Sputtered synthesis of MnO₂ nanorods as binder free electrode for high performance symmetric supercapacitors. *Electrochim. Acta* **2016**, *222*, 1761–1769.
46. Xiong, C.; Li, T.; Dang, A.; Zhao, T.; Li, H.; Lv, H. Two-step approach of fabrication of three-dimensional MnO₂-graphene-carbon nanotube hybrid as a binder-free supercapacitor electrode. *J. Power Sources* **2016**, *306*, 602–610.
47. Cheng, Q.; Tang, J.; Ma, J.; Zhang, H.; Shinya, N.; Qin, L.-C. Graphene and nanostructured MnO₂ composite electrodes for supercapacitors. *Carbon* **2011**, *49*, 2917–2925.
48. Lei, Z.; Zhang, J.; Zhao, X.S. Ultrathin MnO₂ nanofibers grown on graphitic carbon spheres as high-performance asymmetric supercapacitor electrodes. *J. Mater. Chem.* **2012**, *22*, 153–160.
49. Liu, Y.; Hu, M.; Zhang, M.; Peng, L.; Wei, H.; Gao, Y. Facile method to prepare 3D foam-like MnO₂ film/multilayer graphene film/Ni foam hybrid structure for flexible supercapacitors. *J. Alloys Compd.* **2017**, *696*, 1159–1167.
50. Du, L.H.; Yang, P.H.; Yu, X.; Liu, P.Y.; Song, J.H.; Mai, W.J. Flexible supercapacitors based on carbon nanotube/MnO₂ nanotube hybrid porous films for wearable electronic devices. *J. Mater. Chem. A* **2014**, *2*, 17561–17567.
51. Zhang, J.; Zhang, H.L.; Cai, Y.J.; Zhang, H.T. Low-temperature microwave-assisted hydrothermal fabrication of RGO/MnO₂-CNTs nanoarchitectures and their improved performance in supercapacitors. *RSC Adv.* **2016**, *6*, 98010–98017. [[CrossRef](#)]
52. Zhang, Q.; Wu, X.; Zhang, Q.; Yang, F.; Dong, H.; Sui, J.; Dong, L. One-step hydrothermal synthesis of MnO₂/graphene composite for electrochemical energy storage. *J. Electroanal. Chem.* **2019**, *837*, 108–115. [[CrossRef](#)]
53. Fang, T.-Y.; Zeng, Y.-Z.; Liu, Y.-C.; Yang, W.-D. High performance asymmetric supercapacitors fabricated by amorphous MnO₂ on 3D-Ni foam as positive electrodes in a mixed electrolyte. *J. Mater. Sci. Mater. Electron.* **2020**, *31*, 7672–7682.
54. Wang, H.; Fu, Q.; Pan, C. Green mass synthesis of graphene oxide and its MnO₂ composite for high performance supercapacitor. *Electrochim. Acta* **2019**, *312*, 11–21. [[CrossRef](#)]
55. Zhang, J.; Yang, X.; He, Y.; Bai, Y.; Kang, L.; Xu, H.; Shi, F.; Lei, Z.; Liu, Z.H. δ-MnO₂/holey graphene hybrid fiber for all-solid state supercapacitor. *J. Mater. Chem. A* **2016**, *4*, 9088–9096. [[CrossRef](#)]
56. Wang, H.J.; Feng, C.P.; Yu, P.H.; Yang, J. Facile synthesis of MnO₂/CNT nanocomposite and its electrochemical performance for supercapacitors. *Mater. Sci. Eng. B* **2011**, *176*, 1073–1078. [[CrossRef](#)]

